Synthesis and High-Resolution Optical Spectroscopy of Bis(2-(2-thienyl)pyridinato-C^3,N')(2,2'-bipyridine)iridium(III)

Mirco G. Colombo and Hans U. Güdel*

Institut für Anorganische, Analytische und Physikalische Chemie, Universität Bern, Freiestrasse 3, 3000 Bern 9, Switzerland

Received March 10, 1993

The synthesis and high-resolution absorption and luminescence spectra at cryogenic temperatures of $[Ir(thpy)_2bpy]^+$ (thpyH = 2-(2-thienyl)pyridine, bpy = 2,2'-bipyridine) are reported. In the crystalline host lattices $[Rh(ppy)_2bpy]PF_6$ and $[Ir(ppy)_2bpy]PF_6$ (ppyH = 2-phenylpyridine) the lowest excited states around 18 900 cm^{-1} correspond to spin-forbidden $^3\pi-\pi^*$ transitions on the thpy$^-$, whereas the next higher excited state is assigned to an Ir $\rightarrow$ bpy charge-transfer transition at 21 700 cm^{-1}. This metal to ligand charge-transfer (^{3}MLCT) state is found to be strongly dependent on the surroundings. In liquid environments it can shift below the $^3\pi-\pi^*$ state, which remains at about the same energy. Evidence for a mixing of charge-transfer character into the $^3\pi-\pi^*$ excited states is provided by the measured oscillator strengths, the luminescence lifetimes, and the vibronic structure and by a comparison with the properties of analogous cyclometalated Rh^{3+} complexes.

1. Introduction

Excited states of Rh^{3+} and Ir^{3+} chelate complexes with π-accepting ligands are usually classified as ligand centered (LC) $\pi-\pi^*$ or as metal to ligand charge transfer (MLCT).[1-8] This classification is essentially empirical, the luminescence band shape and lifetime being the most important photophysical properties of distinction. The photochemical and photocatalytic properties of such complexes, which are of great current interest,[9,10] are mainly determined by the lowest-energy excited states. We are investigating Rh^{3+} and Ir^{3+} complexes in which it is not a priori clear whether the first excited states have LC or MLCT character. Using the cyclometalating ligands 2-phenylpyridine (ppyH) and 2-(2-thienyl)pyridine (thpyH) besides 2,2'-bipyridine (bpy), it was found that in the mixed-ligand complexes $[Rh(ppy)_2bpy]^+$ and $[Rh(thpy)_2bpy]^+$ the first excited states are localized on the individual ligands and have essentially $^3\pi-\pi^*$ character.[11-17] These results were obtained by using a variety of high-resolution optical spectroscopic techniques[11-16] as well as optically detected magnetic resonance (ODMR).[17] It was found that techniques such as luminescence line narrowing (LLN)[11,12] and particularly absorption spectroscopy with polarized light on single crystals[16] can provide a rather detailed and comprehensive picture of the nature of the relevant excited states.

In the present paper we extend these studies to mixed-ligand cyclometalated Ir^{3+} complexes. The synthesis of $[Ir(thpy)_2bpy]^+$ is described for the first time, and high-resolution optical spectroscopic methods are used to investigate in detail the lowest-energy excited states. We are mainly interested in how the excited-state properties are affected when Rh^{3+} is replaced by Ir^{3+}. The principle of chemical variation has proved to be very important for a thorough understanding of the electronic structure and excited-state properties of such systems. We can learn a great deal if we can follow a trend within a series of related complexes. The mixed-ligand nature of $[Ir(thpy)_2bpy]^+$ is important for three reasons. First, on the basis of our previous work with the corresponding Rh^{3+} complexes, we expect $^3\pi-\pi^*$ and ^{3}MLCT transitions in the same energy range. What are the consequences of this proximity in the Ir^{3+} complex? Is there substantial mixing of LC and MLCT character? Is the classification scheme still valid? Second, the controversal question of localization/delocalization of the excitation can be tackled by polarized absorption spectroscopy. Third, excitation energy transfer between the different ligands can be directly followed by using selective laser excitation.

2. Experimental Section

2.1. Synthesis. The synthesis of $[Rh(ppy)_2bpy]PF_6$, $[Rh(thpy)_2bpy]PF_6$, and $[Ir(ppy)_2bpy]PF_6$ has been described in the literature,[3-5,8] but high-quality compounds can also be obtained by following the alternative procedure given here for $[Ir(thpy)_2bpy]PF_6$.

$[Ir(thpy)_2Cl]_2$ was prepared according to the procedure given in ref 18 with some adaptations as described below. $IrCl_3 \cdot nH_2O$, $n \approx 3$ (1.8 g, Johnson-Matthey), was dissolved in a degassed mixture of water (20 mL) and 2-methoxyethanol (60 mL, Fluka puriss pa). 2-(2-Thienyl)-pyridine (3.1 g, Lancaster Synthesis) was added, and the solution was refluxed under argon at 120 °C for 18 h. After cooling of the solution to room temperature, an aqueous solution of HCl (10 mL, 1.0 M) was added and the reaction mixture was put in the refrigerator for 2 h. The precipitate was collected on a glass filter frit, washed with water and diethyl ether (Merck pa), and dried under vacuum to yield a red-brown powder (2.19 g, 78%). This powder was dissolved in dichloromethane, flash chromatographed over silica gel, precipitated by the addition of *n*-hexane (Merck pa), and collected on a glass filter frit. After washing with diethyl ether and drying under vacuum, $[Ir(thpy)_2Cl]_2$ was obtained as a bright orange powder (1.44 g, 51% with respect to $IrCl_3$).

(1) Carstens, D. H. W.; Crosby, G. A. *J. Mol. Spectrosc.* **1970**, *34*, 113.
(2) Flynn, C. M., Jr.; Demas, J. N. *J. Am. Chem. Soc.* **1974**, *96*, 1959.
(3) Sprouse, S.; King, K. A.; Spellane, P. J.; Watts, R. J. *J. Am. Chem. Soc.* **1984**, *106*, 6647.
(4) Mäder, U.; Jenny, T.; von Zelewsky, A. *Helv. Chim. Acta* **1986**, *69*, 1085.
(5) Ohsawa, Y.; Sprouse, S.; King, K. A.; DeArmond, M. K.; Hanck, K. W.; Watts, R. J. *J. Phys. Chem.* **1987**, *91*, 1047.
(6) Maestri, M.; Sandrini, D.; Balzani, V.; Maeder, U.; von Zelewsky, A. *Inorg. Chem.* **1987**, *26*, 1323.
(7) King, K. A.; Watts, R. J. *J. Am. Chem. Soc.* **1987**, *109*, 1589.
(8) Maeder, U.; von Zelewsky, A.; Stoeckli-Evans, H. *Helv. Chim. Acta* **1992**, *75*, 1320.
(9) Brown, G. M.; Chan, S. F.; Creutz, C.; Schwarz, H. A.; Sutin, N. *J. Am. Chem. Soc.* **1979**, *101*, 7638.
(10) Kirch, M.; Lehn, J. M.; Sauvage, J. P. *Helv. Chim. Acta* **1979**, *62*, 1345.
(11) Colombo, M. G.; Zilian, A.; Güdel, H. U. *J. Am. Chem. Soc.* **1990**, *112*, 4581.
(12) Colombo, M. G.; Zilian, A.; Güdel, H. U. *J. Lumin.* **1991**, *48*, *49*, 549.
(13) Riesen, H.; Krausz, E.; Zilian, A.; Güdel, H. U. *Chem. Phys. Lett.* **1991**, *182*, 271.
(14) Zilian, A.; Güdel, H. U. *Coord. Chem. Rev.* **1991**, *111*, 33.
(15) Zilian, A.; Güdel, H. U. *J. Lumin.* **1992**, *51*, 237.
(16) Frei, G.; Zilian, A.; Raselli, A.; Güdel, H. U.; Bürgi, H. B. *Inorg. Chem.* **1992**, *31*, 4766.
(17) Giesbergen, C. P. M.; Sitters, R.; Frei, G.; Zilian, A.; Güdel, H. U.; Glasbeek, M. *Chem. Phys. Lett.* **1992**, *197*, 451.
(18) Nonoyama, M. *Bull. Chem. Soc. Jpn.* **1979**, *52*, 3749.

0020-1669/93/1332-3081$04.00/0

[Ir(thpy)$_2$bpy]PF$_6$. A mixture of [Ir(thpy)$_2$Cl]$_2$ (220 mg) and molten 2,2′-bipyridine (1.2 g, Fluka puriss pa) were stirred under argon at T = 100 °C for 5 h. After cooling of the solution to room temperature, excess bipyridine was removed by extraction with degassed diethyl ether. The remaining orange precipitate was collected on a glass filter frit, washed with degassed diethyl ether, and dried under vacuum to yield [Ir(thpy)$_2$bpy]Cl (279 mg, 98%). The complex was dissolved in methanol, chromatographed over Sephadex LH 20 (Pharmacia), and converted to the PF_6^- salt by methathesis with NH_4PF_6 (Fluka purum) in methanol (Merck pa) to yield Ir(thpy)$_2$bpy]PF$_6$ (216 mg, 67%). For further purification the complex was recrystallized in acetonitrile (Merck pa) by slow solvent exchange with diethyl ether.

The products were characterized by ^{1}H NMR spectroscopy and powder X-ray diffraction.

The complexes were imbedded in poly(methyl methacrylate) (PMMA) by dissolving the salts in dichloromethane and adding this solution to a solution of 8% PMMA in dichloromethane. The glasses were obtained by slow evaporation of the solvent. Doped crystals were prepared by dissolving the host and guest complex together in dichloromethane or methanol followed by cocrystallization of the complexes by slow solvent exchange with diethyl ether.

2.2. Measurements. ^{1}H NMR spectra were obtained on a Bruker AC-300 FT NMR spectrometer. Dichloromethane-d_2 (Fluka) was used as a solvent.

Cyclic voltammetric measurements were made with a Metrohm E 612 VA scanner, a Metrohm 626 Polarekord, and a Graphtec WX 2400 XY recorder under argon in an airtight one-compartment cell which was equipped with a platinum wire working electrode, a platinum wire counter electrode and a silver/silver chloride reference electrode operating in lithium chloride saturated ethanol. The measurements were done with scan rates of 50 mV/s. The solvents used were acetonitrile or dimethylformamide (Merck pa) both 0.05 M in tetrabutylammonium hexafluorophosphate (Fluka electrochemical grade). The half-wave potential of ferrocenium/ferrocene was used to calibrate the system.

Absorption spectra of solutions were made in a fused silica cell on a Hewlett Packard 8452A diode array spectrophotometer. Luminescence spectra of solutions at room temperature were obtained on a Spex FluoroMax spectrofluorometer which was equipped with a Hamamatsu R928 side window PM tube. For low-temperature measurements the samples were cooled with the helium gas flow tube technique.[19] Luminescence spectra were generally excited with suitable lines of a Spectra Physics 2045 argon ion laser or a Coherent Innova 301-K krypton ion laser. Selective excitations were achieved with a Lambda Physik FL 3002 dye laser, operating with coumarine 152 (Radiant Dyes) and pumped by the 3rd harmonic (355 nm) of a Quanta Ray DCR-3 pulsed Nd:YAG laser. The luminescence was dispersed by two gratings (1200 grooves/mm, blaze at 500 nm) in a 0.85-m Czerny-Turner double monochromator (Spex 1402) and detected by a cooled RCA 31034 end window PM tube connected to a Stanford Research SR 400 photon-counting system. Luminescence lifetimes were measured by chopping the exciting light with a Coherent 305D digital modulation system driven by a Wavetek 802 pulse generator and recording the luminescence decay curves with the RCA 31034 end window PM tube connected via a Stanford Research SR440 preamplifier to a Stanford Research SR430 multichannel scaler. For excitation and single-crystal absorption spectra the light of an Oriel 100-W tungsten lamp, dispersed by two gratings (1200 grooves/mm, blaze at 500 nm) in a Spex Ramalog 0.85-m Czerny-Turner double monochromator was used as a light source. In case of the excitation spectra the luminescence was separated from the exciting light by a cut-off glass filter (Schott OG 570) in the optical path between sample and the detection system, which consisted of a cooled Hamamatsu R3310 PM tube, a Hamamatsu C716 preamplifier, and a Stanford Research SR400 photon-counting system. For single-crystal absorption spectra the light was polarized by a Glan-Taylor polarizer, split into reference and sample beam, detected by a Hamamatsu R928 side window PM tube connected to a Keithley 417 picoammeter and converted to absorbance by a home built double-beam attachment. For monochromator control and data acquisition an IBM AT compatible personal computer was used. With this set-up a resolution of 2 cm^{-1} and an accuracy of about ±2 cm^{-1} in the energy could be reached.

The optical quality of the single crystals was checked by observation of their behavior between crossed polarizers with an Olympus SZ4045 stereo microscope. The crystal dimensions were measured optically with an accuracy of 15 μm. [Ir(ppy)$_2$bpy]PF$_6$ and [Rh(ppy)$_2$bpy]PF$_6$, doped with the title complex, crystallized in pseudohexagonal needles with typical dimensions of about 1 mm × 0.2 mm × 0.1 mm, where the needle axis corresponds to the $\vec{b}$-axis of the orthogonal unit cell.[16] Measurements were made with the light propagating parallel to the $\vec{a}$-, $\vec{b}$-, and $\vec{c}$-axes, respectively. For light propagating along the $\vec{b}$-axis the extinction direction parallel to the lateral crystal faces (1 mm × 0.2 mm) corresponds to the $\vec{a}$- and the extinction direction vertical to the lateral crystal faces to the $\vec{c}$-axis of the unit cell, respectively.

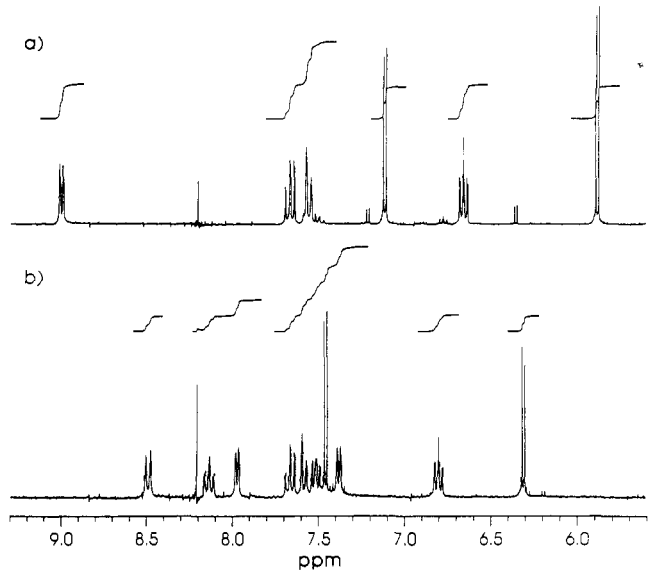

Figure 1. ^{1}H NMR spectra of [Ir(thpy)$_2$Cl]$_2$ (a) and [Ir(thpy)$_2$bpy]$^+$ (b) in CD_2Cl_2 vs tetramethylsilane (TMS).

3. Results

3.1. NMR Spectra and Electrochemistry. The proton NMR spectra of [Ir(thpy)$_2$Cl]$_2$ and [Ir(thpy)$_2$bpy]$^+$ are shown in Figure 1. The spectrum of [Ir(thpy)$_2$Cl]$_2$ in dichloromethane-d_2 shows six resonances in the δ range 5.8–9.0 ppm vs tetramethylsilane (TMS) which can be assigned to the protons of a set of magnetically equivalent cyclometalating thienylpyridine ligands.[18] In the spectrum of [Ir(thpy)$_2$bpy]$^+$ additional resonances in the aromatic region are showing up. With their integrated intensity they can be assigned to a set of four protons. This is only compatible with a molecule possessing a 2-fold axis making the two aromatic rings of the bpy ligand magnetically equivalent.

Ir(thpy)$_2$bpy]PF$_6$ shows a reversible reduction wave at −1750 mV vs ferrocenium/ferrocene ($Fc^{+/0}$) and an oxidation wave at 960 mV vs $Fc^{+/0}$.

3.2. Absorption and Luminescence Properties. The absorption spectra of [Ir(thpy)$_2$Cl]$_2$ and [Ir(thpy)$_2$bpy]PF$_6$ in dichloromethane at room temperature are shown in Figure 2. The absorption spectrum of [Ir(thpy)$_2$Cl]$_2$ shows the following characteristic features: an absorption band at 22 020 cm^{-1} (ϵ = 8900 L mol^{-1} cm^{-1}) and a broad intense band centered at 34 730 cm^{-1} (ϵ = 47 600 L mol^{-1} cm^{-1}). Additionally a shoulder can be located at about 31 240 cm^{-1}. The absorption spectrum of [Ir(thpy)$_2$bpy]PF$_6$ is quite similar but somewhat shifted toward higher energy: The first band is now at 24 000 cm^{-1} (ϵ = 8900 L mol^{-1} cm^{-1}), the second band at 35 800 cm^{-1} (ϵ = 46 300 L mol^{-1} cm^{-1}), and the shoulder at 32 250 cm^{-1} (ϵ = 30 600 L mol^{-1} cm^{-1}). A weak absorption tail (ϵ < 1500 L mol^{-1} cm^{-1}) is observed down to 18 000 cm^{-1} in both spectra.

Figure 3 shows the dependence of the room-temperature luminescence of [Ir(thpy)$_2$bpy]PF$_6$ on the medium. The luminescence spectrum in dichloromethane is characterized by a broad structureless band with its maximum at 16 670 cm^{-1}. The luminescence spectrum in acetonitrile is still dominated by a broad band with its maximum at 16 550 cm^{-1}, but in addition there is a shoulder showing up at about 18 720 cm^{-1}. Imbedding the

(19) Krausz, E.; Tomkins, C.; Adler, H. *J. Phys. E: Sci. Instrum.* **1982**, *15*, 1167.

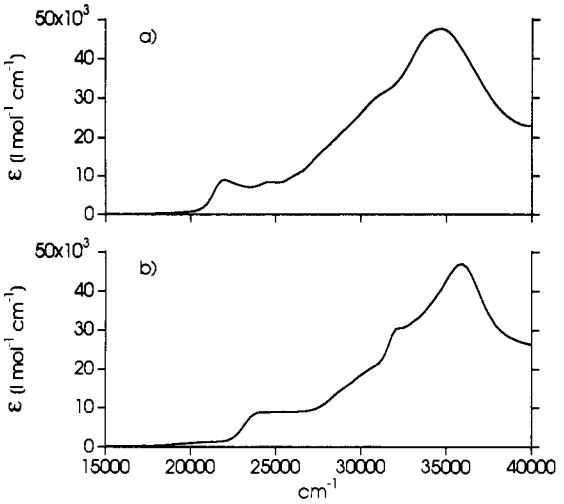

Figure 2. Absorption spectra of $[Ir(thpy)_2Cl]_2$ (a) and $[Ir(thpy)_2bpy]PF_6$ (b) in CH_2Cl_2 at room temperature. The spectra are corrected for the absorption of the solvent.

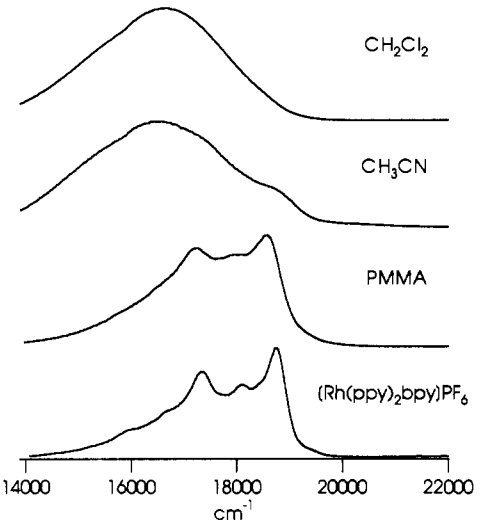

Figure 3. Luminescence spectra of $[Ir(thpy)_2bpy]PF_6$ in different media at room temperature and excitation at 364 nm. The title complex was dissolved in CH_2Cl_2 (10^{-5} M) or CH_3CN (6×10^{-5} M) in case of the upper two spectra and embedded in poly(methyl methacrylate) (PMMA, 10^{-3} M) or doped into the crystal lattice of $[Rh(ppy)_2bpy]PF_6$ (1%) for the lower spectra.

complex into a rigid host drastically changes the shape of the luminescence spectrum. In PMMA it shows a structured band with its highest energy maximum at 18 500 cm^{-1}, close to the position of the shoulder in the acetonitrile spectrum. In the crystalline host $[Rh(ppy)_2bpy]PF_6$ the structure is more pronounced, and the spectrum is blue shifted with the first maximum at 18 700 cm^{-1}.

The temperature dependence of the luminescence spectrum of $[Ir(thpy)_2bpy]PF_6$ in PMMA (a) and $[Rh(ppy)_2bpy]PF_6$ (b) is shown in Figure 4. Between room temperature and 5 K the PMMA spectrum shifts its first maximum toward higher energy by about 120 cm^{-1} and the vibrational structure becomes better resolved. But the width of these vibrational bands is still about 360 cm^{-1} due to inhomogeneous broadening in the glass. In the crystalline sample the blue shift of the first maximum is only 90 cm^{-1} and at 5 K the luminescence lines have a width of less than 6 cm^{-1}.

Polarized single-crystal absorption spectra at T = 9 K of $[Ir(thpy)_2bpy]PF_6$ doped (0.8%) into $[Rh(ppy)_2bpy]PF_6$ are displayed in Figure 5. The two sharp lines at 22 126 and 22 148 cm^{-1}, respectively, which are marked by an asterisk, are the origins of the $[Rh(ppy)_2bpy]PF_6$ host absorption.[16] Here we only describe

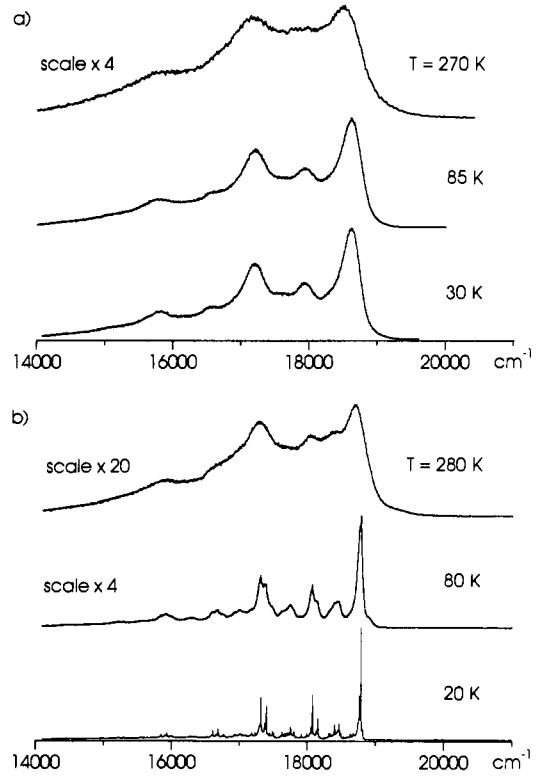

Figure 4. Temperature dependence of the luminescence spectra of $[Ir(thpy)_2bpy]PF_6$ in (a) PMMA (10^{-5} M) and (b) $[Rh(ppy)_2bpy]PF_6$ (1%). The samples were excited with an Ar laser at 363.8 nm (a) or at 457.9 nm (b).

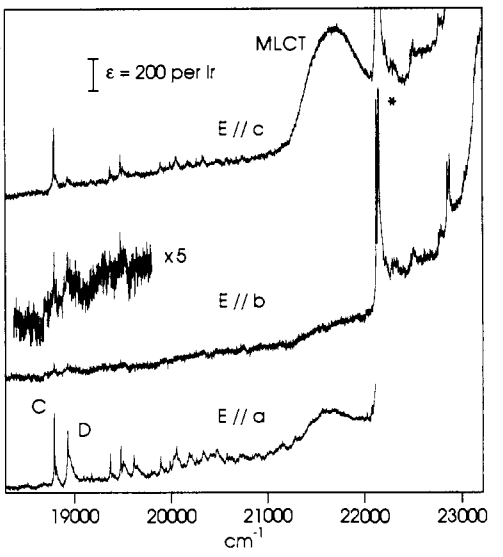

Figure 5. Polarized single-crystal absorption spectra at T = 9 K of $[Ir(thpy)_2bpy]PF_6$, doped into $[Rh(ppy)_2bpy]PF_6$ (0.8%). The spectra were recorded with the electric field vector parallel to the $\vec{a}$-, $\vec{b}$-, and $\vec{c}$-axes of the crystal, respectively. The labels C, D, and MLCT are explained in section 3.2. The asterisk marks the electronic origin of the host.

and discuss the lower energy absorption features which are due to $[Ir(thpy)_2bpy]^+$. There are two sharp origins C and D at 18 789 and 18 928 cm^{-1}, respectively, accompanied by their vibrational sidebands and a broad intense band labeled MLCT with its center at about 21 700 cm^{-1}.

The dichroic ratios of the sharp and broad bands are quite different: While band C is about equally intense for light polarized along the $\vec{a}$- and $\vec{c}$-axes of the crystal, the polarization of the D band is mainly along $\vec{a}$, and the MLCT band is most intense for $E \| \vec{c}$. None of the bands has a significant transition moment along the $\vec{b}$-axis. The extinction coefficients and oscillator strengths of the bands are listed in Table I. An analysis of the intensity

Table I. Extinction Coefficients and Oscillator Strengths of the Lowest-Energy Excitations of $[Ir(thpy)_2bpy]PF_6$ Doped into $[Rh(ppy)_2bpy]PF_6$

	C band			D band			MLCT band	
polarization	ϵ_{max}(origin) (L mol^{-1} cm^{-1})	f(origin)	f(tot. band)	ϵ_{max}(origin) (L mol^{-1} cm^{-1})	f(origin)	f(tot. band)	ϵ_{max} (L mol^{-1} cm^{-1})	f
$\vec{E}\parallel\vec{a}$	470	3.68×10^{-5}	2.46×10^{-4}	325	5.25×10^{-5}	3.50×10^{-4}	130	1.77×10^{-4}
$\vec{E}\parallel\vec{b}$	40	6.38×10^{-6}	4.25×10^{-5}	20	6.26×10^{-6}	4.17×10^{-5}	30	7.71×10^{-5}
$\vec{E}\parallel\vec{c}$	390	4.96×10^{-5}	3.31×10^{-4}	55	1.03×10^{-5}	6.84×10^{-5}	510	1.88×10^{-3}
av	300	3.09×10^{-5}	2.06×10^{-4}	133	2.30×10^{-5}	1.53×10^{-4}	223	7.12×10^{-4}

distribution reveals that the origins C and D carry about 15% of the intensity of the structured absorption.

Figure 6 shows a comparison of the highly resolved low-temperature luminescence spectra of $[Ir(thpy)_2bpy]PF_6$ (a–c) and the analogous $[Rh(thpy)_2bpy]PF_6$ (d and e) in different media. In spectrum a PMMA served as an embedding matrix. In order to reveal the vibrational structure, the luminescence line-narrowing technique (LLN) was applied.[20] In spectra b and d the crystal lattice of $[Rh(ppy)_2bpy]PF_6$ was used as a host, and in spectra c and e the complexes were doped into the isostructural lattice of $[Ir(ppy)_2bpy]PF_6$.[21]

At first sight all the crystal spectra are looking the same. The change of the host or replacement of the metal does not seem to affect the vibrational structure. Upon closer inspection distinct differences between the Rh and Ir spectra become evident: Two vibrational sidebands, one at 297 cm^{-1} and one at 315 cm^{-1} and indicated by arrows in Figure 6, are always present in the spectra of the Ir^{3+} complex but are missing in the spectra of the analogous Rh^{3+} complex. The wing accompanying each sharp line and separated by about 22 cm^{-1} is always more intense in the Ir spectra than in the Rh spectra. Some of the vibrations show small energy shifts up to 11 cm^{-1}, when the coordinated metal is replaced.

Note that the largest energy shifts between the Rh and Ir vibrations is observed in the low-energy vibration ν_3 (Table III). The frequencies of the high-energy vibrations of Rh and Ir are almost identical. In the PMMA spectrum a the sharp lines are accompanied by much more intense phonon sidebands,[20,22] but the energies of the sharp lines are still the same as in the crystal spectra. Note that in spectrum b the complex was selectively excited into the origin D but all the luminescence originates from the origin C.

In Figure 7 a comparison of the 6 K excitation and luminescence spectra of $[Ir(thpy)_2bpy]PF_6$ doped into $[Rh(ppy)_2bpy]PF_6$ is displayed relative to the common origin C. The energy ladders indicate the dominant vibrations (solid lines) and their combination and overtones (dotted and broken lines). The vibrational energies of the investigated complexes are listed in Tables II and III for absorption/excitation and luminescence spectra, respectively.

Neither in the luminescence nor in the excitation spectra do the vibrational energies markedly depend on the surrounding medium. All vibrations have slightly but significantly different energies in the ground and excited states. The additional vibrations ν_1 = 297 cm^{-1} and ν_2 = 315 cm^{-1} observed in the luminescence spectra of $[Ir(thpy)_2bpy]PF_6$ but absent in the spectra of $[Rh(thpy)_2bpy]PF_6$ (cf. Figure 6) can also be seen in the excitation spectra of the former, now at ν_1 = 274 cm^{-1} and ν_2 = 306 cm^{-1}. The splitting between the origins C and D, covering the range from 116 to 218 cm^{-1} for $[Ir(thpy)_2bpy]^+$ and from 156 to 260 cm^{-1} for $[Rh(thpy)_2bpy]^+$, respectively, in the three lattices studied here, is strongly host dependent.

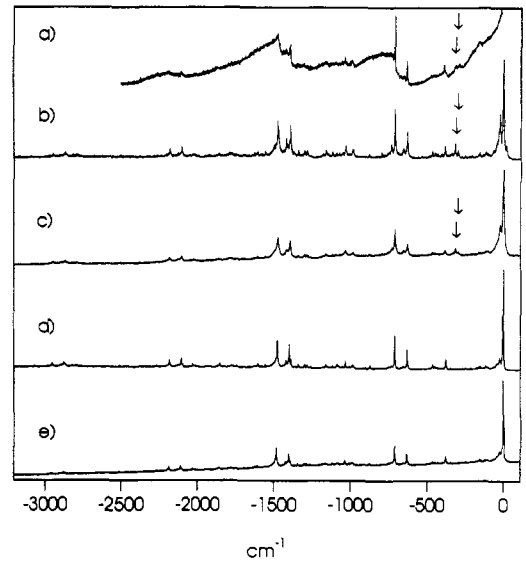

Figure 6. Luminescence spectra of $[Ir(thpy)_2bpy]PF_6$ (a–c) and $[Rh(thpy)_2bpy]PF_6$ (d, e) relative to their origins at T = 6 K. (a) is the luminescence line-narrowing spectrum of $[Ir(thpy)_2bpy]PF_6$ in PMMA, with excitation at 18 832 cm^{-1}. In (b) and (d) the complexes were doped into $[Rh(ppy)_2bpy]PF_6$, and in (c) and (e) $[Ir(ppy)_2bpy]PF_6$ served as a host. Selective excitation into the origin D at 18 928 cm^{-1} was used for spectrum b. The other spectra were excited with the 363.8-nm line of an Ar laser. The arrows indicate two vibrational sidebands, which are always present in the spectra of the Ir^{3+} complex but missing in the spectra of the analogous Rh^{3+} complex.

4. Discussion

4.1. Structural Considerations. In the dichloro-bridged dimer the strong trans influence of the σ-donor carbon leads to a configuration in which the coordinating carbons are trans to the chloro bridge as has already been reported by Nonoyama.[18] This is nicely reflected in the proton NMR spectrum which shows all the four thienylpyridine ligands to be magnetically equivalent. In the monomer this configuration is retained. The bridging chlorides have been replaced by the nitrogens of the bpy, leading to a configuration with the coordinating carbons trans to the nitrogens of the bpy. In this configuration the complex has C_2 symmetry giving rise to 10 resonances in the proton NMR spectrum. This is the same molecular configuration as in $[Rh(thpy)_2bpy]^+$.[8]

The powder X-ray diffraction patterns show that the investigated Ir^{3+} complexes are isostructural to the corresponding Rh^{3+} complexes.[8,16]

4.2. Nature of the Lowest Excited States. A good starting point for the characterization of the lowest excited states is provided by the absorption spectra in Figure 2. The intense bands above 30 000 cm^{-1} can be assigned to spin-allowed ligand-centered transitions (^{1}LC) either on the $thpy^-$ ligands only (a) or on the $thpy^-$ and bpy ligands (b). The absorption bands below 27 000 cm^{-1} are attributed to metal to ligand charge-transfer transitions (MLCT) in accordance with similar spectra reported for $[Rh(thpy)_2bpy]^+$.[6] The lowest MLCT transition of the dimer corresponds to a formal electron transfer from Ir to $thpy^-$, because the accepting orbitals of the chloride lie at higher energy and therefore are not involved. For the monomer, on the other hand,

(20) Personov, R. I. In *Spectroscopy and Excitation Dynamics of Condensed Molecular Systems*; Agranovich, V. M., Hochstrasser, R. M., Eds.; North Holland: Amsterdam, 1983; pp 555–619.
(21) Colombo, M. G. To be published.
(22) Small, G. J. In *Spectroscopy and Excitation Dynamics of Condensed Molecular Systems*; Agranovich, V. M., Hochstrasser, R. M., Eds.; North Holland: Amsterdam, 1983; pp 515–554.
(23) Zilian, A.; Frei, G.; Güdel, H. U. *Chem. Phys.*, in press.
(24) Zilian, A.; Güdel, H. U. *Inorg. Chem.* **1992**, *31*, 830.

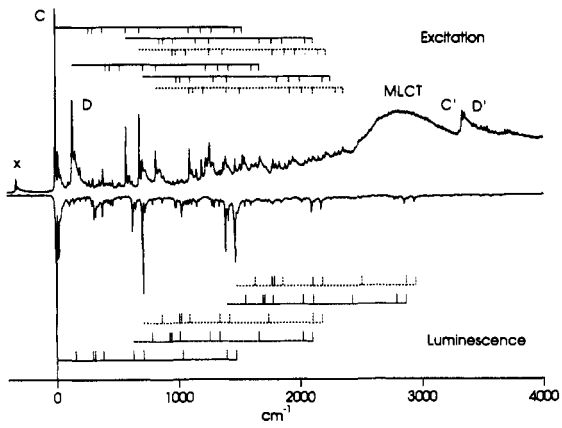

Figure 7. Comparison of the high-resolution excitation (luminescence-monitored broad band below 17 500 cm^{-1}) and luminescence (excitation at 363.8 nm with an Ar laser) spectra of [Ir(thpy)$_2$bpy]PF$_6$ in [Rh(ppy)$_2$bpy]PF$_6$ at T = 6 K. The spectra are displayed relative to their common origin C at 18 789 cm^{-1}. The energy ladders indicate the most intense fundamental vibrations (solid lines) and their combinations and overtones (broken and dotted lines). × is the origin of an unidentified trap.

it is not a priori clear whether the thpy$^-$ or the bpy is involved in the lowest MLCT state. The extinction coefficient of about 9000 L mol^{-1} cm^{-1} for the band at 24 000 cm^{-1} suggests that it belongs to a formally spin-allowed transition. Then the long unstructured tail extending out into the visible region ($\epsilon \approx 1000$ L mol^{-1} cm^{-1} at 20 000 cm^{-1}) could be due to the corresponding spin-forbidden transitions (^{3}MLCT) which have gained intensity by mixing with the allowed transitions through the large spin–orbit coupling of the iridium. The spin-forbidden ligand-centered transitions (^{3}LC) are also expected to lie in this region, probably buried under the more intense MLCT bands. Therefore the question of the nature of the lowest excited state cannot be answered by the solution absorption spectra.

The luminescence spectra of the monomer in different environments as shown in Figure 3 clarify the situation somewhat. Obviously there are two different kinds of emissions: a structured band with its intensity maximum at about 18 700 cm^{-1} and a broad structureless band centered at about 16 600 cm^{-1}. Structured bands with small Stokes shifts are normally attributed to ^{3}LC transitions whereas broad structureless bands with large Stokes shifts can be due either to MLCT or metal-centered (MC) transitions. Here the high ligand field strength of the cyclometalating thpy$^-$ moves the unoccupied metal orbitals to such a high energy that a low-lying MC state can be excluded. MLCT states are known to be strongly solvent dependent whereas LC states are less sensitive to environmental changes. Using the above empirical classification, we conclude that in dichloromethane solution the ^{3}MLCT state is stabilized with respect to the ^{3}LC state but by doping the complex into rigid hosts the charge-transfer transition is moving to higher energy and the ^{3}LC state becomes the lowest excited state. In acetonitrile solution both emissions can be seen simultaneously. We ascribe this to a broad distribution of local environments in solution, leading to two subsets, one with a ^{3}LC and one with a ^{3}MLCT lowest excited state. The well-resolved vibrational structure in the low-temperature luminescence spectra of complexes doped into crystalline or glassy media allows an unambiguous identification of the ligand on which the lowest ^{3}LC state is localized. The vibrational sideband pattern is very specific; it can therefore be used as a fingerprint for the identification of the active ligand.[11,12] On the basis of luminescence line-narrowing,[11,12] hole-burning,[13] Zeeman,[14,15] and optically detected magnetic resonance (ODMR)[17] experiments the lowest excited states of [Rh(thpy)$_2$bpy]$^+$ and [Rh(ppy)$_2$bpy]$^+$ have been assigned to ^{3}LC transitions on the cyclometalating ligands. From the similarity of the sideband patterns in the luminescence spectra of [Rh(thpy)$_2$bpy]$^+$ and [Ir(thpy)$_2$bpy]$^+$ in the same host lattices (Figure 6 and Table III) we conclude that in the Ir^{3+} complex the lowest excited state is also centered on the thpy$^-$ ligand.

Absorption spectra of solutions and glasses reveal no structure in the region of the first ^{3}LC and ^{3}MLCT excitations. In order to get more insight into this spectral region, it is essential to use crystal spectroscopy.[16,25] The inhomogeneous broadening of spectral lines is greatly reduced, and spectra of the quality shown in Figures 5-7 can be obtained. Using single crystals, polarized light, and the knowledge of the crystal structure,[16] we can determine the components of the transition moment with respect to the symmetry axes of the complex. This information is very important for an unambiguous assignment of the excited states. In [Ir(thpy)$_2$bpy]PF$_6$ the optical density of the lowest-energy absorptions is too high to measure neat crystals. We therefore used the isostructural [Rh(ppy)$_2$bpy]PF$_6$ and [Ir(ppy)$_2$bpy]PF$_6$ as host lattices. Both [Rh(thpy)$_2$bpy]PF$_6$ and [Ir(thpy)$_2$bpy]-PF$_6$ can be incorporated, and using the proper concentrations absorption, excitation and luminescence spectra of the highest quality were obtained.

With the identity of the lowest excited state of [Ir(thpy)$_2$bpy]$^+$-doped [Rh(ppy)$_2$bpy]PF$_6$ established as thpy$^-$-centered ^{3}LC from luminescence we can now proceed to higher energies using absorption and excitation spectra. The lowest-energy absorption line is labeled C in Figure 5, and we can identify a second origin D at 139-cm^{-1} higher energy. Both transitions C and D have very similar vibrational sideband patterns, and in close analogy to the corresponding Rh^{3+} system[16] we can assign them to $^3\pi$–π^* excitations on the crystallographically inequivalent thpy$^-$ ligands. Using the known crystal structure of [Rh(ppy)$_2$bpy]PF$_6$ and the procedure given in detail in ref 16, we find that their polarization is within the ligand plane with dominant short-axis character, similar to the complex [Rh(ppy)$_2$bpy]PF$_6$. The broad absorption band centered at 21 700 cm^{-1} which is mainly $E \| \bar{c}$ polarized (see Figure 5) does not occur in the corresponding Rh^{3+} complex. On the basis of this and its shape and intensity, we assign it to a ^{3}MLCT transition. Its polarization behaviour is compatible with a transition moment parallel to the short axis of the bpy ligand. We conclude that it corresponds to an Ir → bpy charge-transfer excitation.

This view is supported by the results of cyclic voltammetric measurements. The first reduction wave of [Ir(thpy)$_2$bpy]$^+$ at −1.75 V vs Fc$^{+/0}$ occurs almost at the same potential as the corresponding wave of [Ir(ppy)$_2$bpy]$^+$ (−1.77 V vs Fc$^{+/0}$), which has been ascribed to the reduction of the bpy.[5] In the same reference the cyclometalating ligands were found to lie at higher potentials because they can be considered as partly reduced. Therefore we also assign the first reduction wave of [Ir(thpy)$_2$bpy]$^+$ to the reduction of the bpy. Within the potential range of our measurements we did not see the reduction waves of the thpy$^-$; they have to occur at higher potentials. The first oxidation wave, ascribed to the oxidation of the Ir^{3+}, is found at slightly higher potential (0.96 V vs Fc$^{+/0}$) than in [Ir(ppy)$_2$bpy]$^+$ (0.86 V vs Fc$^{+/0}$).[5] These results are in good agreement with our assignment of the lowest-energy CT band to an Ir → bpy transition.

We thus have the very interesting situation that the lowest-energy $^3\pi$–π^* excited states are localized on the cyclometalating ligands whereas the lowest-energy ^{3}MLCT excitation corresponds to an Ir → bpy transition. The order of the MLCT transitions correlates with the order of the reduction potentials, in agreement with a simple one-electron picture. The position and relative order of the lowest-energy $^3\pi$–π^* excitations, on the other hand, is determined by other factors and cannot be explained by a one-electron picture. The important interactions here are exchange interactions in the π–π^* excited state which lead to the splitting of approximately 14 000 cm^{-1} between $^1\pi$–π^* and $^3\pi$–π^*. Both in the Rh^{3+} and Ir^{3+} complexes discussed here these interactions

(25) Yersin, H.; Gallhuber, E.; Hensler, G. *Chem. Phys. Lett.* **1987**, *140*, 157.

Table II. Energy of the Origins and of the Dominant Vibrational Sidebands in Absorption/Excitation

Complex	$[Ir(thpy)_2bpy]PF_6$						$[Rh(thpy)_2bpy]PF_6$					
Host	$[Rh(ppy)_2bpy]PF_6$		$[Ir(ppy)_2bpy]PF_6$		$[Rh(thpy)_2bpy]PF_6$		$[Rh(ppy)_2bpy]PF_6$[a]		$[Ir(ppy)_2bpy]PF_6$		neat cyrstal	
Line	C	D	C	D	C	D	C	D	C	D	C	D
Origin [cm^{-1}]	18789	18928	18799	18915	18557*	18775*	19205	19361	19209	19347	18979*	19239*
ν_1	274	271	274	270			---	---				
ν_2	306	309	304				---	---				
ν_3	388	388	386				377	378				
ν_4	580	575	580	572			581	575	572			
ν_5	688	685	688	684			689	685				
ν_6	1102	1097	1102				1101	1097				
ν_7	1201	1207	1204				1207					
ν_8	1288	1281	1286				1288	1281				
ν_9	1477	1474	1477				1483	1476				
ν_{10}	1539	1544	1541	1539			1544	1539				

* Maxima of the inhomogeneously broadened origins. [a] Reference 24.

Table III. Energy of the Origins and the Dominant Vibrational Sidebands in Luminescence

Complex	$[Ir(thpy)_2bpy]PF_6$			$[Rh(thpy)_2bpy]PF_6$		
Host	$[Rh(ppy)_2bpy]PF_6$	$[Ir(ppy)_2bpy]PF_6$	PMMA	$[Rh(ppy)_2bpy]PF_6$[a]	$[Ir(ppy)_2bpy]PF_6$	PMMA
Origin [cm^{-1}]	18789	18799	*	19205	19209	*
ν_1	297	298	294	---	---	---
ν_2	315	315	314	---	---	---
ν_3	383	385	384	376	376	383
ν_4	629	632	630	630	632	636
ν_5	710	713	709	711	713	714
ν_6	1033	1034	1033	1032	1034	1036
ν_7	1395	1396	1394	1399	1401	1402
ν_8	1473	1475	1476	1479	1481	1483

* Luminescence line narrowing experiment: vibrational energies are given relative to the exciting laser line. [a] Reference 25.

are stronger for $\pi-\pi^*$ excitations on thpy$^-$ than on bpy, pushing the thpy$^-$-centered $^3\pi-\pi^*$ states to the lowest energy.

Figure 5 is very instrumental in arriving at these conclusions. It is to our knowledge the first spectrum in which both LC and MLCT transitions are clearly identifiable with their respective transition moment directions. In order to obtain the relevant information we need high spectral resolution, cryogenic temperatures, and single crystals with a known structure. These are not routine experiments, but the present study shows that on a well-chosen system the considerable effort to obtain these spectra can be worthwhile.

4.3. Mixing between the LC and MLCT Excited States. The oscillator strengths of the absorption bands in Figure 5 are in a range ($f = 10^{-3}$–10^{-5}; see Table I) which is characteristic for ^{3}MLCT transitions ($[Os(bpy)_3]$: $f \approx 6 \times 10^{-3}$ per bpy, estimated from refs 26 and 27). The oscillator strength of the transition C can be correlated with the radiative luminescence lifetime. Assuming an electric dipole (ed) intensity mechanism, it is given as[28]

$$[f_{ij}(\mathrm{ed})]\tau = 1.5 \times 10^4 \frac{\lambda_0^2}{n[^1/_3(n^2+2)]^2} \quad \text{(SI units)} \qquad (1)$$

where τ is the radiative lifetime, n the refractive index of the substance, and λ_0 the vacuum wavelength of the transition.

The total oscillator strength $f_{ij}(\mathrm{ed})$ for an electric dipole allowed transition between the states i and j is defined as

$$f_{ij}(\mathrm{ed}) = {}^1/_3[f_{ij}^x(\mathrm{ed}) + f_{ij}^y(\mathrm{ed}) + f_{ij}^z(\mathrm{ed})] \qquad (2)$$

where f_{ij}^q is the oscillator strength for a transition with q polarized light. The oscillator strength of an absorption band can be deduced from the spectrum according to[29]

$$f_{ij}^q = 4.32 \times 10^{-9} \int_{\text{abs band}} \epsilon(\bar{\nu})\, \mathrm{d}\bar{\nu} \qquad (3)$$

where $\epsilon(\bar{\nu})$ is the extinction coefficient in q polarization and the energy scale is in cm^{-1}. In case of a triply degenerate excited and a nondegenerate ground state the oscillator strengths deduced from the absorption spectra have to be divided by three to calculate proper lifetimes from eq 1. In $[Ir(thpy)_2bpy]^+$-doped $[Rh(ppy)_2bpy]PF_6$ the three spin sublevels of the excited state C are equally populated at the experimental temperature of 10 K and we estimate the refractive index to be 1.5.

The calculated lifetime of the luminescent band C thus calculated using eq 1 is 21 μs, which compares very well with the experimental lifetime $\tau_{exp} \approx 17$ μs at $T = 10$ K. This means that at 10 K the lifetime is determined by the radiative decay and consequently the quantum yield is close to one. The weak temperature dependence of the luminescence intensity from the $[Ir(thpy)_2bpy]^+$-doped $[Rh(ppy)_2bpy]PF_6$ crystal supports this argument: from 6 K up to 200 K the luminescence intensity only decreases by about 25% implying that nonradiative decay processes play only a subordinate role in this temperature range.

From the observed absorption intensities in Figure 5 we estimate that the oscillator strength of the Ir → bpy charge-transfer transition is about three times bigger than the oscillator strengths of the C and D transitions. It thus appears that the ligand-centered $^3\pi-\pi^*$ transitions have acquired considerable charge-transfer character. This is supported by their in-plane polarization on the one hand and by comparison with the corresponding $[Rh(thpy)_2bpy]^+$ complex. In the latter the luminescence lifetime at 77 K was found to be 500 μs,[6] which, according to eq 1, corresponds to an oscillator strength $f = 8.1 \times 10^{-6}$, between 1 and 2 orders of magnitude smaller than in the Ir^{3+} complex. This difference can be ascribed to the larger spin–orbit coupling parameter for Ir^{3+} on the one hand and the proximity of the intensity donating

(26) Felix, F.; Ferguson, J.; Güdel, H. U.; Ludi, A. *Chem. Phys. Lett.* **1979**, *62*, 153.
(27) Pankuch, B. J.; Lacky, D. E.; Crosby, G. A. *J. Phys. Chem.* **1980**, *84*, 2061.
(28) Imbusch, G. F. In *Luminescence Spectroscopy*; Lumb, M. D., Ed.; Academic Press: London, 1987; pp 1–92.
(29) Schäfer, H. L.; Gliemann, G. *Einführung in die Ligandenfeldtheorie*; Akademische Verlagsgemeinschaft: Frankfurt a. M., Germany, 1967; p 92.

MLCT states on the other. It should be noted, however, that the transitions C and D, being localized on the two $thpy^-$ ligands cannot, in first order, steal their intensity from the lowest-energy Ir → bpy CT transition but from unobserved higher-lying Ir → $thpy^-$ CT transitions.

There are two other observables which are fully compatible with the stronger CT character of the C and D excited states in $[Ir(thpy)_2bpy]^+$. The first is the occurrence in the high-resolution luminescence and excitation spectra (Figures 6 and 7) of two lines at 297 and 315 cm^{-1} and at 274 and 306 cm^{-1}, respectively, which are absent in the spectra of the corresponding Rh^{3+} complex. These two vibrations occur in a spectral range where we expect metal–ligand bending and stretching modes.[30,31] The occurrence of metal–ligand sidebands in nominally ligand-centered transitions is thus a manifestation of their increased charge-transfer character. All the lines in the luminescence and excitation spectra of Figures 6 and 7 carry a phonon sideband, which is separated by about 22 cm^{-1} and which is significantly more intense for $[Ir(thpy)_2bpy]^+$ than $[Rh(thpy)_2bpy]^+$. This phonon sideband is a measure of the coupling of the chomophore or luminophore to its environment, usually called electron–phonon coupling.[20,22] MLCT excitations are known to be more strongly dependent on the environment than LC excitations.[24] It therefore makes intuitive sense that the higher intensity of the phonon sidebands for transitions C and D in $[Ir(thpy)_2bpy]^+$ is a reflection of their stronger CT character.

It is remarkable that the overall appearance of the C and D bands is still that of organic $^3\pi-\pi^*$ transitions. Their total intensity, on the other hand, is increased by 3 orders of magnitude compared to the free ligand.[6] It appears, therefore, that the substantial charge-transfer character of these excitations directly affects the intensities and thus lifetimes but has only a minor effect on their band shape and intensity distribution.

(30) Nakamoto, K. *Infrared and Raman Spectra of Inorganic and Coordination Compounds*; 4th ed.; Wiley-Interscience: New York, 1986; pp 208–213.

(31) Strommen, D. P.; Malick, P. K.; Danzer, G. D.; Lumpkin, R. S.; Kincaid, J. R. *J. Phys. Chem.* **1990**, *94*, 1357.

5. Conclusions

By using high-resolution optical spectroscopy, it was possible to characterize the lowest-energy excited states in the mixed-ligand complex $[Ir(thpy)_2bpy]^+$. Crystal spectra obtained with polarized light were used to identify the ligand on which the lowest-energy excited states C and D are localized. As in the corresponding $[Rh(thpy)_2bpy]^+$ complex, they are localized on the cyclometalating $thpy^-$ ligands. For the first time the lowest-energy MLCT transition could be observed in the same absorption spectrum. It lies only about 2900 cm^{-1} above the first excited state, and it was identified as an Ir → bpy CT transition. In the corresponding $[Rh(thpy)_2bpy]^+$ complex this transition has not been observed so far; it must therefore lie at considerably higher energy. Several indications were found that the first excited states C and D have more CT character in $[Ir(thpy)_2bpy]^+$ than in $[Rh(thpy)_2bpy]^+$. In fluid media at room temperature the luminescence of $[Ir(thpy)_2bpy]^+$ has the typical shape and Stokes shift of a charge-transfer band and is red-shifted with respect to the crystal spectra; see Figure 3. We ascribe this to a reversal of the order of the first $^3\pi-\pi^*$ and ^{3}MLCT excited states in the different environment. The red-shift is an indication that the MLCT state has shifted to lower energy. It is generally accepted that MLCT transitions depend more strongly on the molecular environment than $^3\pi-\pi^*$ transitions. Since the first ^{3}MLCT excited state was identified as Ir → bpy in the crystal spectra, the luminescence in solution is most likely due to a Ir → bpy charge-transfer process. The acetonitrile solution shows two types of luminescence, one with a typical CT shape and the weaker one with the $^3\pi-\pi^*$ shape. We believe that this is the result of a broad inhomogeneous distribution of complex sites in the solution. This results in two sets of complexes, one set with the first ^{3}MLCT below the $^3\pi-\pi^*$ and a minority set with the opposite ordering.

Acknowledgment. We thank Gabriela Frei for helpful discussions and the group of Dr. P. Bigler for the NMR service. $IrCl_3$ was generously provided as a loan by Johnson-Matthey. Financial support by the Swiss National Science Foundation is gratefully acknowledged.